A Novel Ultra-Wide-Band Transmitarray Design Using Tightly Coupled Dipole Elements

Yuanming Cai, *Member, IEEE*, Wenting Li, Ke Li, *Member, IEEE*, Seven Gao, *Member, IEEE* and Yinzeng Yin, *Member, IEEE*

***Abstract*—A novel design of transmitarray (TA) antenna based on tightly coupled dipole array is presented in this paper. The array consists of 20×10 unit cells, and each unit cell is composed of a pair of short dipoles connected with a section of meandered transmission line (TL). The size of each unit cell is 20 mm×10 mm, which is about 0.2λ×0.1λ, where λ is the wavelength in free space at the lowest working frequency of the TA. By introducing the mutual coupling between adjacent units of the TA, the bandwidth of the TA can be improved dramatically. Due to the wideband characteristics of both the tightly coupled dipole array and meandered TLs, the proposed TA is able to achieve ultra-wide bandwidth performance. To verify the design concept, a prototype of the proposed TA is fabricated and measured. A log-periodic dipole antenna is used as the feed antenna of the TA. The measured results agree with the simulated results well. The operational band of the prototype is from 3 GHz to 9.5 GHz. Within the working band of the TA antenna, the radiation pattern is stable and the main beam of the antenna is not distorted or split. It is the first time that the TA based on tightly coupled dipole array is reported.**

***Index Terms*—transmitarray, wideband antenna, tightly coupled arrays, ultra-wide-band antenna**

I. Introduction

TRANSMITARRAYS (TAs) are planar discrete lenses that operate a phase-front transformation by converting an incident spherical wave front into an outgoing plane wave propagating in a specified direction. As a kind of high gain antenna, TA has many advantages, such as the low profile, lightweight, easy fabrication, low cost and no feed blockage[1].

A TA antenna consists of an illuminating feed source and a flat transmitting surface composed of an array of unit cells. The feed source is usually located at the equivalent focal point of the transmitting surface. The transmission phase of each unit cell in TA is individually designed to convert the spherical phase front from the feed to a planar phase front. As a result, a focused radiation beam can be realized with a high gain[2].

There are two different techniques for TA designs. One approach involves using multilayer frequency selective surfaces (M-FSSs). This approach uses frequency selective surface (FSS) as "free-space phase shifter" to obtain the desired phase delays to form the focused beam [3-6]. However, a full 360° phase range compensation cannot be obtained by only one layer of the printed FSS[7]. Thus, multilayer design in which the layers are separated by either air gaps or dielectric laminates is required to increase the transmission phase range of the antenna element [8]. In [9], two layers of modified Malta crosses connected by four vias are used. The bandwidth of the TA based on the M-FSS depends on the bandwidth of M-FSS. Although this TA unit cell has a small thickness, it has a relatively narrow bandwidth. Higher order FSS with multi-layer structure can increase the bandwidth [10, 11]. In [10], six layers of patches are used to design a wideband bandpass FSS for wide band TA. In [12] and [13], four layers or five layers of patches are used for wide band TAs. The transmission phase can be controlled by adjusting the lengths of patches. Two metallic layers of double-ring slots [14] and four layers of split ring slots [15] have been used as high order FSS for the design of wideband TAs. The transmission phases of those TA units are controlled by adjusting the sizes the slots. The TA reported in [16] has three layers of three-dipole element. By adjusting the lengths of dipoles and the widths of gaps between adjacent dipoles, a 300° phase range compensation can be achieved. In [17], three layers of stacked ring resonators with stubs are used. The stubs' length are used to control the transmission phase. In [18], a semi-planar TA with varied number of metal layers is reported. The layer number and patterns on layers in the each unit-cell are optimized for wideband characteristic. Although higher order FSSs can improve the bandwidths of the TAs, they increase the synthesis and fabrication complexity.

Another way to design TA is using "receive-transmit (R-T)" configuration. One array antenna receives the signal from the feed antenna and transmits to another array antenna with proper phase shift to compensate the spatial phase delay [19-23]. In [20], aperture coupled microstrip patches with stripline delay lines are used as receiving and transmitting antennas. The transmission phase can be controlled by adjusting the length of the stripline. In [21], probe feed microstrip patches with microstrip feed line are used to design TA. The transmission phase can be controlled by adjusting the length of the

This work was supported in part by the China Postdoctoral Science Foundation under Grant 2016M602769, the Fundamental Research Funds for the Central Universities under Grant JBX170215.

Yuan-Ming Cai and Yingzeng Yin are with the National Key Laboratory of Antennas and Microwave Technology, Xidian University, Xi'an, Shaanxi, 710071, China. (e-mail: ymcai@xidian.edu.cn).

W. Li, and S. Gao are with the School of Engineering and Digital Arts, University of Kent, Canterbury CT2 7NT, U.K.

Ke Li is with the School of Information Science and Technology, Northwest University, Xi'an, Shaanxi, 710127, China

microstrip line. In [22], the TA unit cell consists of two identical square back-to-back microstrip patch antennas, and they are connected by a via. The transmission phase can be controlled by rotating the patch on the top layer. In [23], stacked patches based on proximity-coupled feeding are used as array antenna, and two bridged-T shifters in each unit are used to achieve over 400° phase range. Due to the narrow bandwidth of the radiating element and the insertion loss, the reported TAs in those papers using this approach usually have narrow bandwidths.

To design a wideband TA, the tightly coupled dipole array (TCDA) is adopted in this paper. This is inspired by the wideband planar low-profile TCDA antennas [24, 25] and tightly coupled dipole reflectarray [26]. By introducing the capacitive coupling between dipoles, the bandwidth increases and the profile of the TCDA can be reduced [25]. In this paper, the concept of TCDA are used to extend the operational band of TA unit and a novel ultra-wide-band TA is proposed. The tightly coupled dipoles are used as TA elements for good transmission coefficient magnitude within a wide band. The meandered parallel microstrip lines are used as true time delay lines to compensate the spatial phase delay.

As the TCDA is used to form a TA antenna, the proposed TA antenna combines the advantages of both TCDAs and TA antennas. The proposed antenna features a wider operational band compared with other planar TA antennas, and a simpler feed network compared with TCDAs. In its operational band, the unidirectional radiation pattern is stable. To our best knowledge, this work is the first one investigating the tightly coupled TA.

This paper is organized as follows. The geometry and characteristics of the proposed unit-cell and TA are presented in Section II. This study also includes a theoretical discussion on the phase of transmission coefficient of the TA element as a function of frequency, aiming to improve the bandwidth of the TA. Section III presents the design of the TA antenna, as well as the simulation and measurement results. Section VI concludes this paper.

II. Wideband TA Theory and Design

In this section, the concept of equivalent distance delay is introduced to design the required unit-cell elements of the UWB TA. Then the proposed TA unit is presented and analyzed. At last, a UWB TA prototype operating from 3 GHz to 9.5 GHz is designed.

A. Required Spatial Phase Shift for Wideband TAs

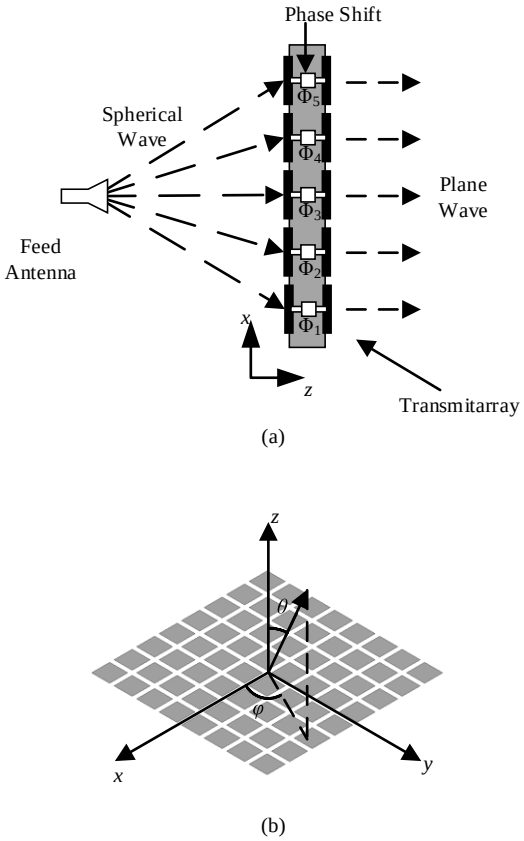

Fig. 1. (a) The configuration of a typical TA, and (b) its coordinate system

The configuration of a typical TA and its coordinate system are shown in Fig. 1. The position of an element on the TA surface is (x_i, y_i), and the distance between this element and the position of the feed antenna is R_i. The phase of transmission coefficient of the TA element is $\Phi_i(x_i, y_i)$, and $\varphi_i(x_i, y_i)$ is the phase distribution across the array aperture, then,

$$\varphi_i(x_i, y_i) = \Phi_i(x_i, y_i) - R_i k_0 + \Phi_{FS}(\theta_i, \varphi_i) + \varphi_0 \quad (1)$$

Where k_0 is the wave number in the free space. $\Phi_{FS}(\theta_i, \varphi_i)$ is the phase of the focal source radiation pattern in the direction of unit cell i. φ_0 is a phase constant that can be added to all elements of the array.

On the other hand, if the beam direction of the TA is (θ_b, φ_b), and using a simple linear phase distribution across the array aperture, the required phase distribution across the array aperture can be rewritten as follow:

$$\varphi_i(x_i, y_i) = -k_0 \sin\theta_b (x_i \cos\theta_b + y_i \sin\varphi_b) \quad (2)$$

By considering the equation (1) and (2), the required phase shift for each unit cell, which provides necessary phase compensation, is derived as follow:

$$\Phi_i(x_i, y_i) = -k_0 \sin\theta_b (x_i \cos\theta_b + y_i \sin\varphi_b) - \varphi_0 + R_i k_0 - \Phi_{FS}(\theta_i, \varphi_i) \quad (3)$$

For a TA antenna, even if the beam direction (θ_b, φ_b), the positions of the TA elements (x_i, y_i), and the position of the feed antenna are kept unchanged, $\Phi_i(x_i, y_i)$ varies with frequency. In order to eliminate the effects of frequency, equation (3) is

divided by k_0, then

$$\frac{\Phi_i(x_i,y_i)}{k_0} = -\sin\theta_b\left(x_i\cos\theta_b + y_i\sin\varphi_b\right) + R_i - \frac{\varphi_0 + \Phi_{FS}(\theta_i,\varphi_i)}{k_0} \quad (4)$$

If the position of the feed antenna is the phase center of the focal source, $\Phi_{FS}(\theta_i,\varphi_i)$ is independent of i, and $\frac{\varphi_0 + \Phi_{FS}(\theta_i,\varphi_i)}{k_0}$ is independent of i.

Let

$$d_i = \Phi_i(x_i,y_i)/k_0 \quad (5)$$

$$d_i' = d_i - d_1 \quad (6)$$

Then

$$d_i' = -\sin\theta_b\left[(x_i - x_1)\cos\theta_b + (y_i - y_1)\sin\varphi_b\right] + (R_i - R_1) \quad (7)$$

Here d_i refers to the required distance delay of a TA element, and d_i' is the renormalized distance delay. From the right part of the equation (6), the renormalized distance delay d_i', which is the difference between required equivalent distance delay of ith element and that of 1st element, is determined by the beam direction (θ_b, φ_b), the positions of the TA elements (x_i, y_i) and the position of the feed antenna. d_i' is independent of the frequency.

If the value of the calculated renormalized distance delay d_i' of the TA element is not change with frequency in a certain band, it means the TA element can compensate differential spatial phase delay within the band. In the next subsection, the wideband TA units is introduced.

B. *Design of the TA Units*

As the insertion losses and the differential spatial phase compensations of TA units determine the performance of the entire TA, two aspects are considered when we design the unit cells of the TA. Firstly, to broaden the range of passband of the TA units with low insertion loss, the tightly coupled dipoles are used. Secondly, true time distance delay lines are used to compensate the spatial phase delays within a wideband.

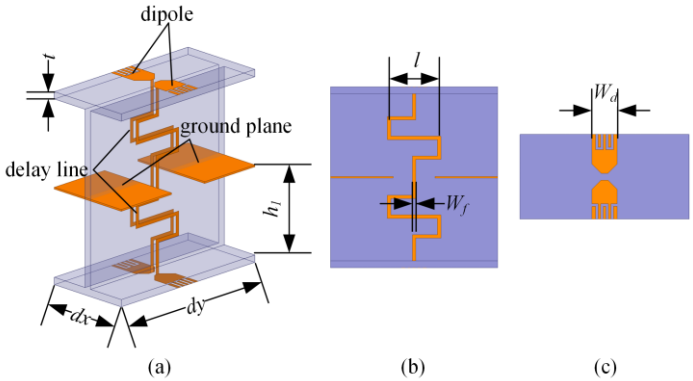

Fig. 2. Geometry of the proposed TA element: (a) side view, (b) front view, and (c) top view.

The side view, front view, and top view of the unit cell are shown in Fig. 2. The geometry of the element is symmetrical about its center. The TA element consists of two dipoles, a delay line, and a ground plane. The dipoles are printed on the surfaces of two Rogers RO4003C substrates with the thickness of t. The interdigital capacitor are introduced between adjacent dipoles. The ground of dipoles consists of two metal strips. The distance between the ground and the dipoles are h_1. By optimized the size of interdigital capacitor and the value of h_1, good transmission coefficient magnitude within a wide operational band can be obtained.

Two pairs of dipoles are connected by the delay line, which is comprised of a pair of meandered parallel microstrip lines. The delay line is printed on two sides of a Rogers RO4003C substrate. The width of the parallel microstrip line is W_f, and the total length of the meandered parallel microstrip lines equal to $4\times l+2\times h_1$. Once the operational band of the element is optimized, the value of h_1 is fixed, and by altering the value of l, the total length of the delay line can be controlled. The detail parameters of the TA element are shown in Table I.

Table I Parameter of the TA element (Unit: mm)

Symbol	Value	Symbol	Value	Symbol	Value
t	0.813	h_1	10	W_f	0.4
d_x	10	d_y	20	W_d	3

There are two steps to design the element of the TA, which will be demonstrated in details.

1) Design of the TCDA element

The proposed TA elements are based on TCDA. The analyzed tightly coupled dipole excited by a lump port is shown in Fig. 3. Similar with the design in [27], the radiator is an interdigital capacitor coupled dipole. The tightly mutual coupling generated by the interdigital capacitors between adjacent elements is critical to the performance of the TA element. It will help to enhance the impedance bandwidth. A metal ground plane is placed under the dipole. The distance between dipole and ground is essential to determine the working band of the elements. The size and structure of the dipole, and the impedance of the lump port are simulated with the help of ANSYS HFSS and optimized for good impedance matching within a wide operational band.

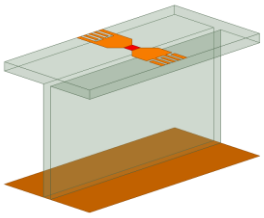

Fig. 3. TCDA element excited with lump port

Fig. 4 shows the simulated VSWR of the tightly coupled dipole element in Fig. 3. The impedance of the lump port is optimized to be 170Ω. The operational band for VSWR<2 is from 3.18 GHz to 9.54 GHz. The height of the element and the minimum distance between adjacent elements are 10 mm, which is only about 1/10 free wavelength at its lowest working frequency 3.18 GHz.

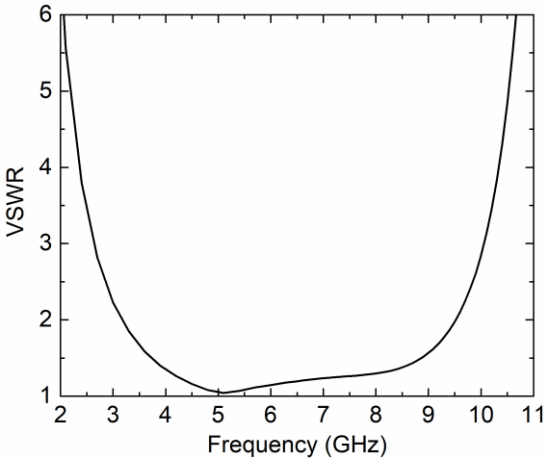

Fig. 4. Simulated VSWR for geometry of Fig. 3

2) Design of tightly coupled dipoles connected with mender delay line

Once the TCDA element is optimized in last step, the structure of the dipole is fixed and two dipoles mounted on two sides of the ground plane are used as receiving element and radiation element in each TA unit as shown in Fig. 2. The two dipoles are then connected with a pair of parallel microstrip lines which works as a balanced transmission line. The pair of parallel microstrip lines work as a true time delay line for necessary phase compensation. In this way, the receiving element can transfer the energy received from the feed antenna to the delay line when the antenna array is illuminated by the feed antenna. Then the energy is continually transferred from the delay line to the radiation element.

The ground plane consists of metal strips is used as shown in Fig 2 instead of a whole metal plane as shown in Fig 3 in order to accommodate the phase delay lines. Thus, the meandered parallel microstrip line can go through the ground plane via the gap between two metal strips. The gap between two metal strips is only 5 mm wide which is about 0.16 wavelength in free space at 9.5 GHz (the highest working frequency in this design). The printed metal strips works as a polarizer. The printed dipoles are aligned parallel to the metal strips and the radiation from the dipoles is reflected by the printed metal strips. Therefore, the metal strip is equivalent to the surface of metal plane in such a way.

The parallel microstrip line is composed of two sections of U-shaped mender line. The characteristic impedance of the parallel microstrip transmission line equals to the optimized impedance 170Ω in last step for better impedance match between TCDA element and delay line. Considering the thickness and permittivity of the substrate, the width of the delay line can be calculated to be 0.4 mm. The substrate which parallel microstrip line are printed on is perpendicular to the orientation of the dipole. As the parallel microstrip line is perpendicular to the orientation of the dipole, the space electromagnetic coupling between the dipole and the transmission line can be avoided. The total length of delay line in the unit is equal to $4\times l+2\times h_1$. By adjusting the length of l, the total length of delay line can be easily controlled. It should be noted that in this design, only two U shaped mender lines are used, more than two section of meander lines can be used for a large adjusting range of the total length.

To test the performance of the TA unit cell, the magnitudes of transmission coefficients with different values of l varying from 1mm to 7mm with 1mm step are calculated as shown in Fig. 5. It can be seen that the magnitudes of transmission coefficients with different values of l are relatively flat within a wideband, and the insertion loss is less than 2 dB within the bandwidth of 3-9.5 GHz for different values of l. Good transmission coefficient magnitude within a wideband is obtained.

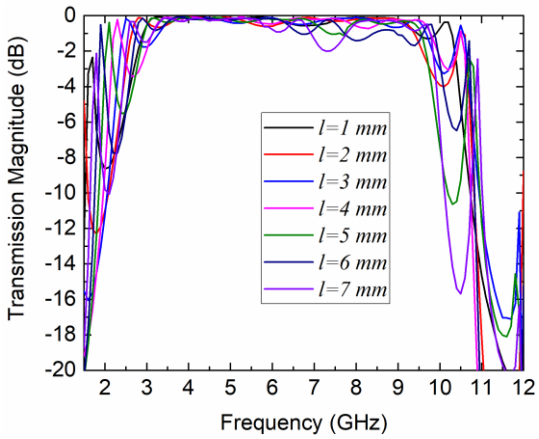

Fig. 5. Caculated transmission coefficient magnitudes against frequency for different geometry of unit cell.

The calculated transmission phase of the elements Φ are shown in Fig. 6. The renormalized equivalent distance delay $d'(l, f)$ produced by the TA unit at different frequencies are also calculated according to equation (5) and (6), and illustrated in Fig. 7, where $d'(l, f)=d(l, f)-d(l_1, f), l_1=1mm$. The calculated transmission phase of the element Φ is varying with frequency f and parameter l dramatically as shown in Fig. 6. However, d' vs. l curves with different frequencies are almost overlapped as shown in Fig. 7. Although the renormalized equivalent distance delays of the proposed unit for different frequencies are not the same precisely, the deviations are very small, which means the proposed element can approximately satisfy equation (7) within a wide frequency range.

A function of $d'(l)$ is desired to design a TA. Here, 2nd-degree polynomial curve fitting in a least-squares sense is used to determine the function of $d'(l)$. The software Matlab is used to do the polynomial curve fitting. The frequency range is set to be from 3GHz to 9 GHz with 1 GHz step, and parameter l is from 1mm to 7mm with 1mm step. So there are 7 frequency samples and 7 parameter l samples, and the total samples of $d'(l, f)$ is 7×7. The function $d'(l)$ is derived to be as follow:

$$d'(l) = -0.0546\times l^2 - 12.5\times l + 12.6 \quad (8)$$

The curve of $d'(l)$ is drawn by small circle in Fig. 7. We can see the residual error is very small. Therefore the function of $d'(l)$ is used to calculate the parameter of l for each TA unit.

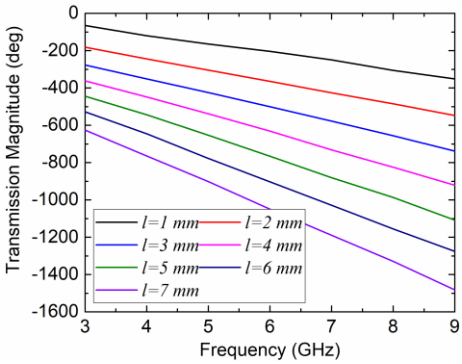

Fig. 6. Caculated transmission coefficient phases against frequency for different geometries of unit cell.

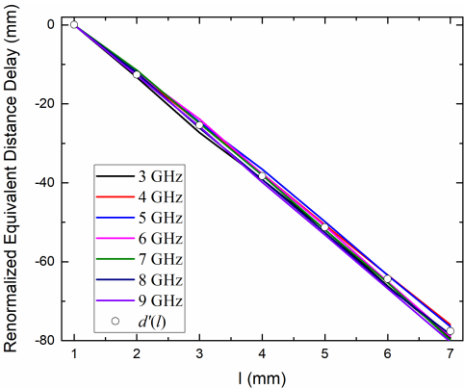

Fig. 7. Caculated renormalizeed equivanalent distance delay of the proposed unit cell.

C. *Design of the Feed Antenna*

A wideband log-periodic dipole antenna (LPDA) is used as the feed antenna [28]. The LPDA antenna is composed of dipoles and a pair of parallel microstrips. It is printed on a Rogers RO4003C substrate with thickness of 0.813 mm. The configuration of the LPDA is shown in Fig. 8.

The structure of the LPDA satisfies the following equation:

$$\frac{l_1}{l_2} = \frac{W_1}{W_2} = k \quad (9)$$

And the parameters of the geometry are listed in table II.

Table II Parameter of the LPDA (Unit: mm)

Symbol	Value	Symbol	Value
l_1	32 mm	k	1.15
w_1	4 mm	tanα	0.46

The phase center of the LPDA changes with frequency. In the TA antenna design, the phase center of LPDA at 6 GHz is posited at the focus point of the TA.

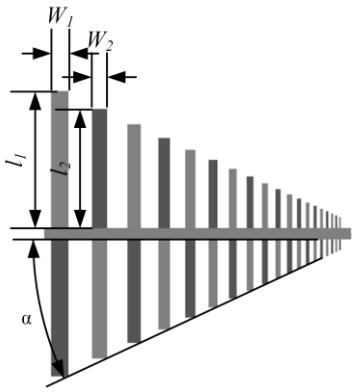

Fig. 8 configure of the feed antenna.

D. *Design of the transmitarray*

The proposed TA consists of 20×10 proposed units. The dimension of the TA is 200×200×21.626mm^3. The focal length of the TA is chosen to 112mm. And the distance between the TA and LPDA feed antenna is 93 mm. The required renormalized distance delay is calculated according to equation (7). In this design, it should be note that 1st element is chosen to be the unit at the corner of the TA and the TA is designed to be a broadside array, R_1 in equation (7) is the distance between the focus to the center of the corner element. Therefore the required distance delay of the 1st element is set to be 0mm, and the required parameter of l of the 1st element is set to be 1mm as well. The calculated renormalized distance delay of each unit of the TA is shown in Fig. 9(a). By using equation (8), the required parameter of l of each element in TA can be derived as shown in Fig. 9(b).

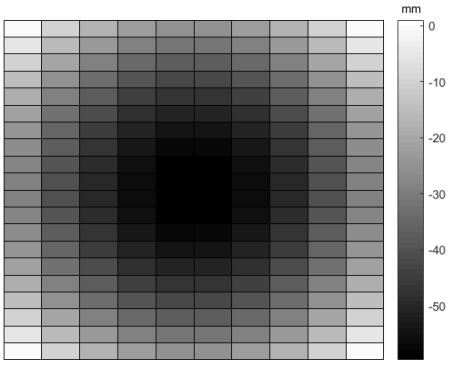

(a)

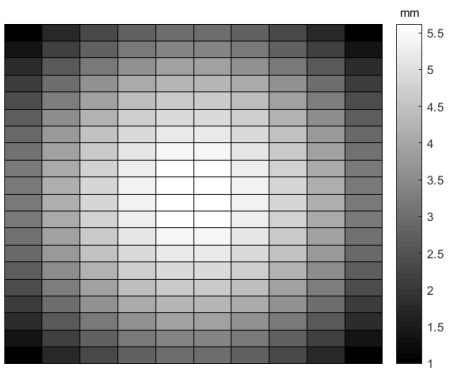

(b)

Fig. 9. Required (a) equivalent distance delay and (b) parameter of *l* for each element in TA.

The configuration of the proposed UWB TA antenna is shown in Fig. 10. The feed antenna is allocated beyond the TA. The phase center of the feed antenna is placed at the focus of the TA and the beam of feed antenna is directed to the center of the TA.

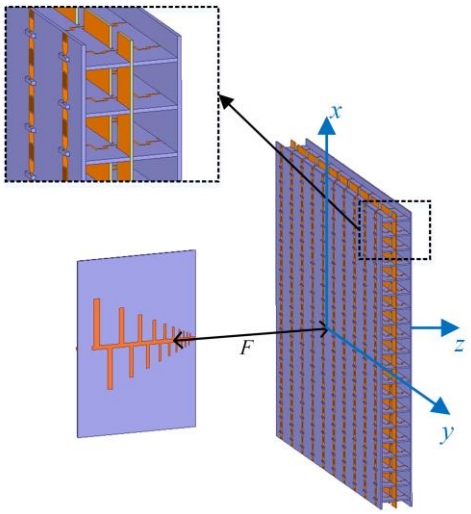

Fig. 10. The configuration of the proposed UWB TA antenna.

III. Simulation and Measurement Results

The proposed ultra-wide-band TA antenna is simulated with full-wave simulation software ANSYS Electronics Desktop.

To better explain the mechanism of the TA antenna, the electrical near field distributions around the TA antenna and corresponding far field 3D radiation patterns at different frequencies are plotted in Fig. 11 and 12, respectively. As shown in Fig. 11, the TA converts an incident spherical wave from the feed antenna into an outgoing quasi plane wave propagating in broadside direction at both higher frequency and lower frequency. As predicted, broadside pencil beams are observed at both frequencies as shown in Fig. 12. It should be noted that the gains of the TA antenna are different at two frequencies as the electrical sizes of array at two frequencies are different.

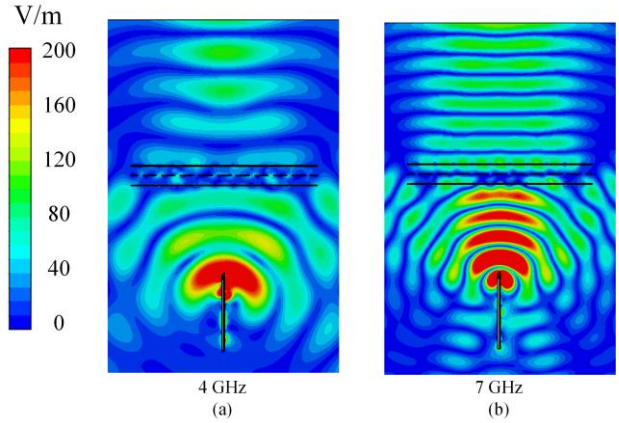

Fig. 11. Simulated electric field contours on a cutting surface in the YOZ-plane at frequency of (a) 4 GHz (b) 7GHz

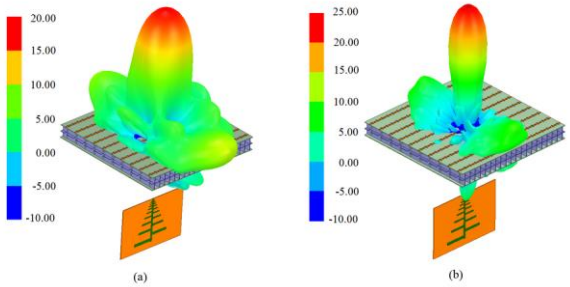

Fig. 12 Simulated 3D radiation pattern at frequency of (a) 4 GHz (b) 7GHz

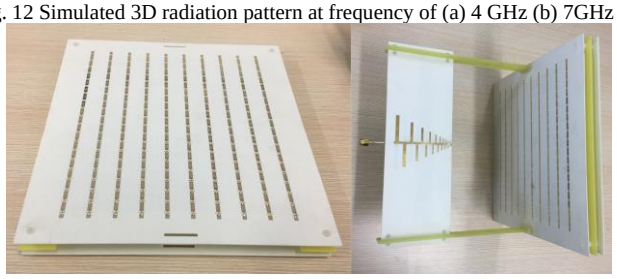

Fig. 13. The picture of the fabricated UWB transmitarray antenna.

To verify our design concept, a prototype of proposed TA antenna is fabricated as shown in Fig. 13. The radiation patterns and gains were measured in an anechoic chamber and the S parameters were measured with a vector network analyzer.

The simulated and measured radiation patterns are shown in Fig. 14. Good agreement between simulation and measurement results is observed. The radiation patterns are stable within a wide band. The radiation pattern is not distorted within the frequency range from 3 GHz to 9.5 GHz. The highest sidelobe level (SLL) in H plane is about -8.4 dB, and the SLL in E plane is about -13.0 dB. The large side lobe around 60° is due to the spillover from the effects of over-illumination of the main transmitarray surface. Fig 15 shows the measured and simulated $|S_{11}|$ of the feed antenna.

The simulated and measured gains of the proposed transmitarray antenna are shown in Fig. 16. The simulated gain varies from 13.78 dBi to 20.36 dBi, while the measured gain varies from 13.3 dBi to 20.6 dBi in the operational band. The measured peak gain is 20.6 dB at 8 GHz. The aperture efficiency AE is calculated using

$$AE = \frac{G}{D_{\max}} \ , \quad D_{\max} = \frac{4\pi A}{\lambda_0^{\ 2}} \tag{10}$$

where G is the measured gain, D_{max} is the maximum directivity, A is the physical area of the antenna aperture, and λ_0 is the free-space wavelength. The simulated and measured aperture efficiencies (AEs) are plotted in Fig. 17. The simulated AEs are over 21% within the working frequency from 3 GHz to 9.5 GHz. The measured AEs are over 20%. The lower AE values are mainly due to the spillover effect. For easy fabrication and low cast, the LPDA antenna is used as feed antenna. However, it has a relatively larger beamwidth in its H plane result in over-illumination. In the future, an ultra-wide-band feed antenna with stable phase centre and suitable radiation pattern can be used as feed antenna to improve the performance of the TA.

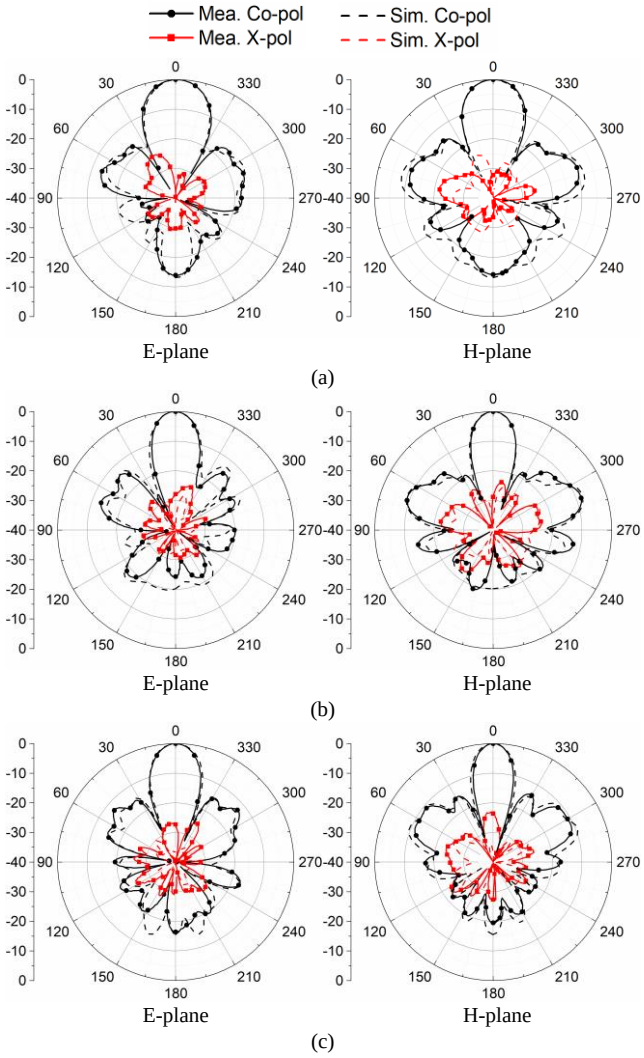

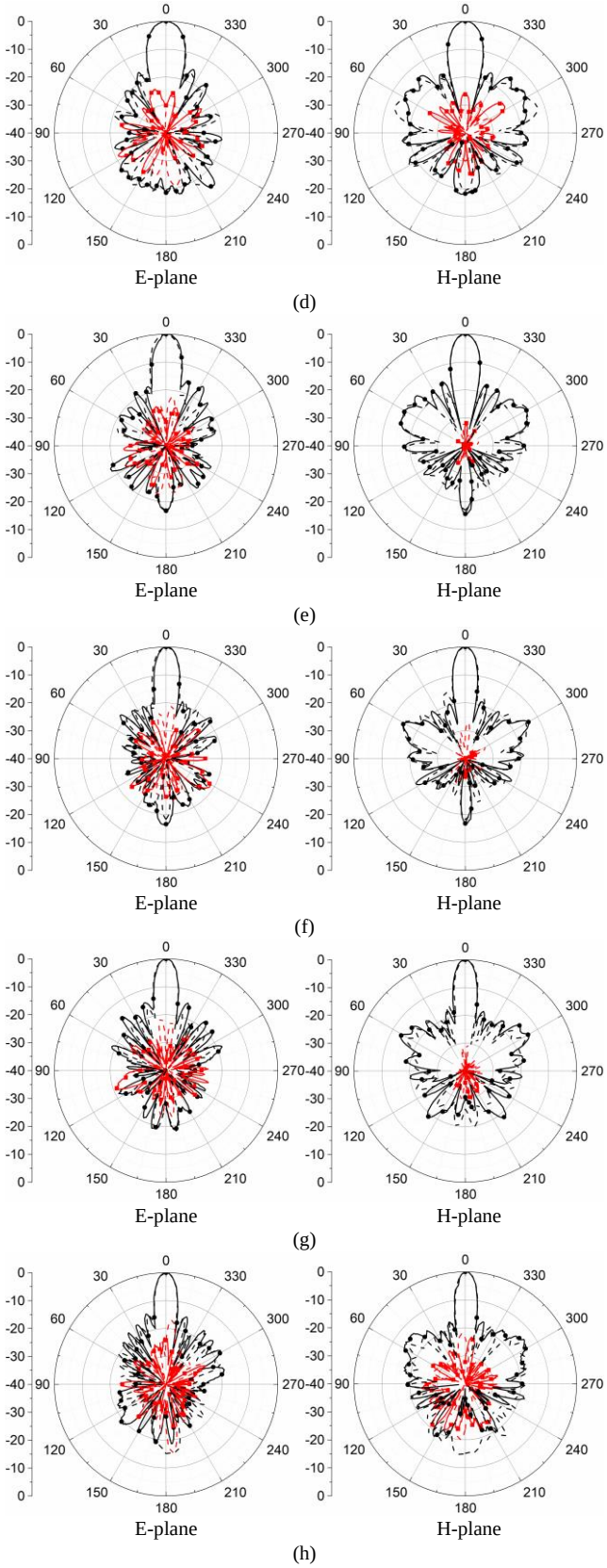

Fig. 14. Radiation patterns of the proposed antenna. (a) 3GHz. (b) 4GHz. (c) 5 GHz. (d) 6 GHz. (e) 7 GHz. (f) 8 GHz. (g) 9 GHz. (h) 9.5 GHz.

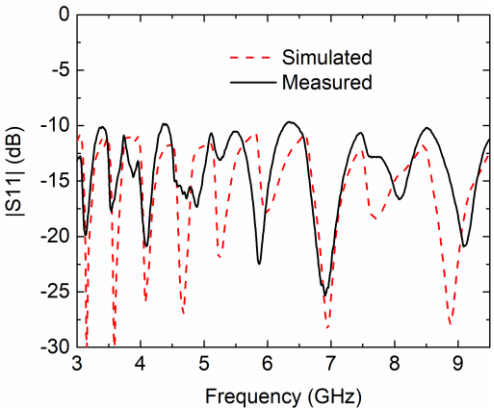

Fig. 15. Simulated and measured S11 of the feed antenna.

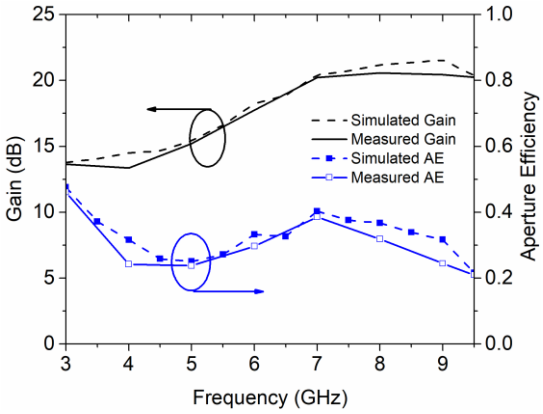

Fig. 16. Simulated and measured antenna gains and aperture efficiency

Some representative works published in the literatures using M-FSS and receive-transmit (R-T) scheme are summarized together in Table III. The definitions of bandwidth used are different among the listed works. We present their achieved fractional bandwidths based on what are presented in their papers. The table III cannot provide a quantitative comparison but rather a qualitative comparison to help the readers to evaluate different TAs. All of the presented works have good beam characteristics with reasonable side lobe levels within their frequency bands. It can be seen that, the proposed antenna has the largest working bandwidth with reasonable gain.

Table III

COMPARISON BETWEEN REPORTED and Proposed TA antennas

Ref.	Bandwidth	Max aperure effeiciency	Configuration of layers	Gain	approach
[5]	5.7%	38%	3 stacked patches	23	M-FSS
[10]	16%	60%	A pair of 3 stacked patches	22	M-FSS
[13]	20%	23.4*18.6cm	5 stacked patches	9.6 dB	M-FSS
[18]	24.27 %	62%	5 stacked ring with air gap	22.3	M-FSS
[19]	15.8%	52.9%	Patch-ground-patch	22.7	R-T
[21]	/	(5.4lambda * 5.4lambda)	Stack patch –mirostrip fed line- stacked patch	23	R-T
[22]	7%	61	Patch-ground-patch	23	R-T
Proposed	104%	46%	Tightly couple dipoles-ground-Tightly couple dipoles	20.36	R-T

IV. CONCLUSION

A novel ultra-wide-band TA has been proposed in this paper. A new unit-cell configuration with two printed tightly coupled dipoles and a pair of meandered parallel microstrip lines has been proposed. The unit cell shows good characteristics including good transmission coefficient magnitudes and applicable spatial phase delay compensation within a wideband. Moreover, the fabrication process of the unit cell relies on standard PCB technologies, which makes the corresponding TA very attractive for low-cost integration. A prototype of the proposed transmitarray is fabricated and measured. The antenna has stable radiation pattern within a wide operational band from 3GHz to 9.5 GHz. The measured gain and aperture efficiency in the operational band are from 13.3 dBi to 20.6 dBi and from 20% to 46%, respectively. Such characteristics make the proposed TA very promising for high-data rate communications.

[1] L. Dussopt, "Transmitarray Antennas," in Signals and Communication Technology, Aperture Antennas for Millimeter and Sub-Millimeter Wave Applications, A. Boriskin and R. Sauleau, Eds., 1st ed.: Springer, 2018. [Online]. Available.

[2] A. H. Abdelrahman, P. Nayeri, A. Z. Elsherbeni, and F. Yang, "Analysis and design of wideband transmitarray antennas with different unit-cell phase ranges," in *2014 IEEE Antennas and Propagation Society International Symposium (APSURSI)*, 2014, pp. 1266-1267.

[3] H. Nematollahi, J.-J. Laurin, J. E. Page, and J. A. Encinar, "Design of Broadband Transmitarray Unit Cells With Comparative Study of Different Numbers of Layers," *IEEE Transactions on Antennas and Propagation*, vol. 63, no. 4, pp. 1473-1481, 2015.

[4] C. Pfeiffer and A. Grbic, "Millimeter-Wave Transmitarrays for Wavefront and Polarization Control," *IEEE Transactions on Microwave Theory and Techniques*, vol. 61, no. 12, pp. 4407-4417, 2013.

[5] B. Rahmati and H. R. Hassani, "Low-Profile Slot Transmitarray Antenna," *IEEE Transactions on Antennas and Propagation*, vol. 63, no. 1, pp. 174-181, 2015.

[6] H.-X. Xu, T. Cai, Y.-Q. Zhuang, Q. Peng, G.-M. Wang, and J.-G. Liang, "Dual-Mode Transmissive Metasurface and Its Applications in Multibeam Transmitarray," *IEEE Transactions on Antennas and Propagation*, vol. 65, no. 4, pp. 1797-1806, 2017.

[7] A. H. Abdelrahman, A. Z. Elsherbeni, and F. Yang, "Transmission Phase Limit of Multilayer Frequency-Selective Surfaces for Transmitarray

Designs," *IEEE Transactions on Antennas and Propagation*, vol. 62, no. 2, pp. 690-697, 2014.

[8] L. Boccia, I. Russo, G. Amendola, and G. Di Massa, "Multilayer Antenna-Filter Antenna for Beam-Steering Transmit-Array Applications," *IEEE Transactions on Microwave Theory and Techniques*, vol. 60, no. 7, pp. 2287-2300, 2012.

[9] W. An, S. Xu, F. Yang, and M. Li, "A Double-Layer Transmitarray Antenna Using Malta Crosses With Vias," *IEEE Transactions on Antennas and Propagation*, vol. 64, no. 3, pp. 1120-1125, 2016.

[10] Q. Luo, S. Gao, M. Sobhy, and X. Yang, "Wideband Transmitarray With Reduced Profile," *IEEE Antennas and Wireless Propagation Letters*, vol. 17, no. 3, pp. 450-453, 2018.

[11] A. H. Abdelrahman, P. Nayeri, A. Z. Elsherbeni, and F. Yang, "Bandwidth Improvement Methods of Transmitarray Antennas," *IEEE Transactions on Antennas and Propagation*, vol. 63, no. 7, pp. 2946-2954, 2015.

[12] T. Cai, G.-M. Wang, X.-L. Fu, J.-G. Liang, and Y.-Q. Zhuang, "High-Efficiency Metasurface with Polarization-Dependent Transmission and Reflection Properties for Both Reflectarray and Transmitarray," *IEEE Transactions on Antennas and Propagation*, pp. 1-1, 2018.

[13] M. A. Al-Joumayly and N. Behdad, "Wideband Planar Microwave Lenses Using Sub-Wavelength Spatial Phase Shifters," *IEEE Transactions on Antennas and Propagation*, vol. 59, no. 12, pp. 4542-4552, 2011.

[14] Y. Chen, L. Chen, J.-F. Yu, and X.-W. Shi, "A C-Band Flat Lens Antenna With Double-Ring Slot Elements," *IEEE Antennas and Wireless Propagation Letters*, vol. 12, pp. 341-344, 2013.

[15] G. Liu, H.-j. Wang, J.-s. Jiang, F. Xue, and M. Yi, "A High-Efficiency Transmitarray Antenna Using Double Split Ring Slot Elements," *IEEE Antennas and Wireless Propagation Letters*, vol. 14, pp. 1415-1418, 2015.

[16] A. Aziz, F. Yang, S. Xu, and M. Li, "An Efficient Dual-Band Orthogonally Polarized Transmitarray Design Using Three-Dipole Elements," *IEEE Antennas and Wireless Propagation Letters*, vol. 17, no. 2, pp. 319-322, 2018.

[17] C. Pfeiffer and A. Grbic, "Planar Lens Antennas of Subwavelength Thickness: Collimating Leaky-Waves With Metasurfaces," *IEEE Transactions on Antennas and Propagation*, vol. 63, no. 7, pp. 3248-3253, 2015.

[18] S. H. Ramazannia Tuloti, P. Rezaei, and F. Tavakkol Hamedani, "High-Efficient Wideband Transmitarray Antenna," *IEEE Antennas and Wireless Propagation Letters*, pp. 1-1, 2018.

[19] A. Clemente, L. Dussopt, R. Sauleau, P. Potier, and P. Pouliguen, "Wideband 400-Element Electronically Reconfigurable Transmitarray in X Band," *IEEE Transactions on Antennas and Propagation*, vol. 61, no. 10, pp. 5017-5027, 2013.

[20] D. M. Pozar, "Flat lens antenna concept using aperture coupled microstrip patches," *Electronics Letters*, vol. 32, no. 23, 1996.

[21] P. Padilla, A. Muñoz-Acevedo, and M. Sierra-Castañer, "Passive microstrip transmitarray lens for Ku band," in *Proceedings of the Fourth European Conference on Antennas and Propagation*, 2010, pp. 1-3.

[22] H. Kaouach, L. Dussopt, J. Lanteri, T. Koleck, and R. Sauleau, "Wideband Low-Loss Linear and Circular Polarization Transmit-Arrays in V-Band," *IEEE Transactions on Antennas and Propagation*, vol. 59, no. 7, pp. 2513-2523, 2011.

[23] J. Y. Lau and S. V. Hum, "A Wideband Reconfigurable Transmitarray Element," *IEEE Transactions on Antennas and Propagation*, vol. 60, no. 3, pp. 1303-1311, 2012.

[24] J. A. Kasemodel, C.-C. Chen, and J. L. Volakis, "Wideband Planar Array With Integrated Feed and Matching Network for Wide-Angle Scanning," *IEEE Transactions on Antennas and Propagation*, vol. 61, no. 9, pp. 4528-4537, 2013.

[25] I. Tzanidis, K. Sertel, and J. L. Volakis, "UWB Low-Profile Tightly Coupled Dipole Array With Integrated Balun and Edge Terminations," *IEEE Transactions on Antennas and Propagation*, vol. 61, no. 6, pp. 3017-3025, 2013.

[26] W. T. Li, S. Gao, L. Zhang, Q. Luo, and Y. M. Cai, "An Ultra-Wide-Band Tightly Coupled Dipole Reflectarray Antenna," (in English), *Ieee Transactions on Antennas and Propagation*, vol. 66, no. 2, pp. 533-540, Feb 2018.

[27] S. S. Holland and M. N. Vouvakis, "The Planar Ultrawideband Modular Antenna (PUMA) Array," *IEEE Transactions on Antennas and Propagation*, vol. 60, no. 1, pp. 130-140, 2012.

[28] C. Campbell, I. Traboulay, M. Suthers, and H. Kneve, "Design of a stripline log-periodic dipole antenna," *IEEE Transactions on Antennas and Propagation*, vol. 25, no. 5, pp. 718-721, 1977.